Environmental Science & Technology

Article

pubs.acs.org/est

Relative Permeability Experiments of Carbon Dioxide Displacing Brine and Their Implications for Carbon Sequestration

Jonathan S. Levine,*[,†,§] David S. Goldberg,[‡] Klaus S. Lackner,[†] Juerg M. Matter,[‡,∥] Michael G. Supp,[§] and T. S. Ramakrishnan[§]

[†]Department of Earth and Environmental Engineering, Columbia University, New York, New York 10027, United States

[‡]Lamont Doherty Earth Observatory, Columbia University, Palisades, New York 10964, United States

[§]Schlumberger-Doll Research, Cambridge, Massachusetts 02143, United States

Supporting Information

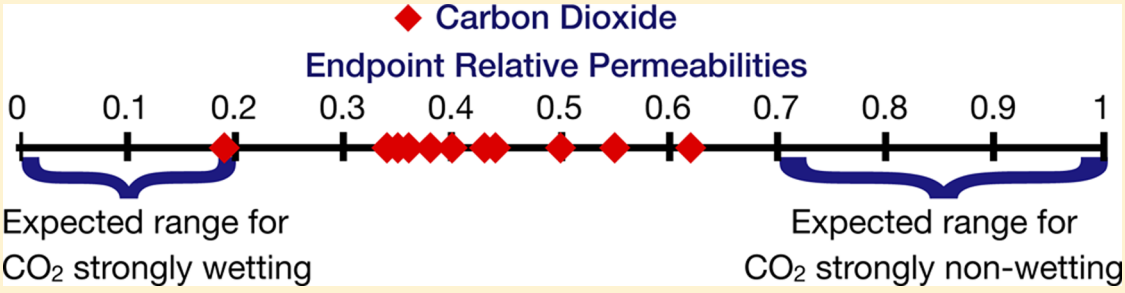

ABSTRACT: To mitigate anthropogenically induced climate change and ocean acidification, net carbon dioxide emissions to the atmosphere must be reduced. One proposed option is underground CO_2 disposal. Large-scale injection of CO_2 into the Earth's crust requires an understanding of the multiphase flow properties of high-pressure CO_2 displacing brine. We present laboratory-scale core flooding experiments designed to measure CO_2 endpoint relative permeability for CO_2 displacing brine at in situ pressures, salinities, and temperatures. Endpoint drainage CO_2 relative permeabilities for liquid and supercritical CO_2 were found to be clustered around 0.4 for both the synthetic and natural media studied. These values indicate that relative to CO_2, water may not be strongly wetting the solid surface. Based on these results, CO_2 injectivity will be reduced and pressure-limited reservoirs will have reduced disposal capacity, though area-limited reservoirs may have increased capacity. Future reservoir-scale modeling efforts should incorporate sensitivity to relative permeability. Assuming applicability of the experimental results to other lithologies and that the majority of reservoirs are pressure limited, geologic carbon sequestration would require approximately twice the number of wells for the same injectivity.

INTRODUCTION

Carbon dioxide capture and sequestration has been proposed to alleviate carbon dioxide emissions from release into the atmosphere, typically by injection into the Earth's crust.[1,2] Only a limited amount of CO_2 can be disposed of in hydrocarbon-bearing strata while increasing hydrocarbon production; therefore, large-scale geological CO_2 disposal will require injection into brine-filled permeable strata. To maximize disposal capacities and minimize the risk of buoyancy-driven leakage through overlying impermeable strata, it is expected that these reservoirs will need to be at high pressures, i.e., large depths, to ensure high CO_2 densities. Therefore, reservoir pressures are expected to be substantially larger than the CO_2 critical pressure of 7.39 MPa. Because of the geothermal gradient, most reservoirs at the necessary pressures will be at temperatures greater than the CO_2 critical temperature of 31.1 °C, though subseabed and subpermafrost reservoirs may be at lower temperatures at which CO_2 would be liquid. Of particular interest are sediments[3] and basalt[4] underlying the deep ocean (>2.7 km depth) where liquid CO_2 is denser than overlying ocean and pore waters and will be trapped by buoyancy.[5] Thus, the reported set of experiments focuses on injection at a pressure, 10 MPa, equivalent to 1 km depth, that ensures a dense CO_2 phase but is within the equipment limitations, with liquid CO_2 experiments at 20 °C and supercritical CO_2 experiments at 50 °C.

Endpoint Relative Permeability. Neglecting body forces, Darcy's law as modified for multiphase flow[6] defines relative permeability and is given by

$$\mathbf{v}_j = -\frac{k k_{rj}(S_j)}{\mu_j}\nabla P_j \tag{1}$$

where k is the intrinsic permeability of the porous medium, and for each phase j, $\mathbf{v}_j$ is the velocity, $k_{rj}(S_j)$ is the relative

Received: April 9, 2013
Revised: November 18, 2013
Accepted: November 25, 2013
Published: November 25, 2013

permeability at saturation S_j, μ_j is the shear coefficient of viscosity, and P_j is the phase pressure. For two phase flow the phases are typically denoted by replacing j with w and n, i.e., the wetting and nonwetting phases, respectively. With two fluid phases saturating the porous medium $S_w = 1-S_n$. $k_{rj}(S_j)$ accounts for the reduction in effective permeability for phase j relative to the intrinsic permeability due to the presence of an additional phase. k_{rj} varies between zero at residual saturation, S_j^o, defined as the saturation at which the fluid being displaced becomes disconnected and thus can no longer flow, and unity when no other phase is present, i.e. $k_{rj}(S_j^o) = 0$, and $k_{rj}(1) = 1$.

The maximum k_{rj} for an invading fluid is limited by an immobile residual amount of the displaced fluid (subscript d) which stops flowing at its residual saturation, S_d^o, and is defined as the endpoint relative permeability, $k_{rj}^o = k_{rj}(S_d^o)$. k_{rj}^o is determined by fluid occupancy at the pore and subpore scales due to capillarity.[7,8] k_{rn}^o is typically in the 0.7−1 range because the residual wetting phase remains at least on parts of the pore walls and in the smallest pores, blocking the smallest fluid pathways that least contribute to flow. Conversely, k_{rw}^o is in the 0.1−0.3 range because the residual nonwetting phase blocks the largest pathways that most contribute to flow. I.e. k_{rj}^o is measuring the multiphase fluid network that results from pore-scale fluid/fluid-rock surface chemistry interactions. Therefore, unlike measurements of k_{rj} at lower intermediate saturations, k_{rj}^o measures a fundamental fluid/fluid-rock property, providing a qualitative measure of in situ wettability. Furthermore, because capillarity determines both k_{rj}^o and pore-scale fluid occupancy at lower S_j, the entire k_{rj} curve is similarly scaled at lower S_j.[7,8] Numerical reservoir codes commonly model k_{rj} with parametrized curves such as the modified Corey curve, with $k_{rj}(S_j)$ directly proportional to k_{rj}^o.[9−12] Ramakrishnan and Wasan[13] provide a percolation theory justification of the relative permeability-saturation-capillary pressure relationship and the Brooks and Corey curve. Thus, our emphasis here is on the determination of the endpoint CO_2 relative permeability, k_{rc}^o, measured at residual saturation of the displaced aqueous phase, S_a^o.

Relative Permeability and Carbon Sequestration. In analyzing the geological suitability of a reservoir for carbon sequestration several factors are of critical importance: CO_2 injection rate, disposal capacity, and lateral and vertical containment, all of which are affected by relative permeability. The elevation of the injection pressure over the reservoir pressure is limited by the pressure at which fracturing occurs in either the target stratum or the overlying mechanical caprock, with a suitable safety factor. This fracturing pressure limit determines the maximum CO_2 injection rate, and for pressure-limited reservoirs the disposal capacity,[14] in direct proportion to relative permeability through eq 1. Injectivity of CO_2 also affects the areal spreading and migration of the CO_2 plume,[15,16] which may need to be laterally restricted due to, e.g., a finite-area overlying impermeable seal, the need to avoid leakage pathways, or area-limited pore space rights; see, e.g., ref 17. More generally, the dynamics and therefore the migration of CO_2 are dictated by the ratio of mobilities of the CO_2 and aqueous phases (denoted by subscripts c and a), $M \equiv \lambda_c/\lambda_a$, where the mobility of each phase is defined as $\lambda_j = kk_{rj}/\mu_j$ and incorporates all fluid-specific parameters in eq 1. As a consequence, in addition to topographic and geological data, reservoir modeling for CO_2 injection requires accurate multiphase flow experimental data, including the endpoint CO_2 relative permeability used to model k_{rc} at lower saturations.

Previous experimental studies report maximum measured k_{rc} outside of the 0.7−1 range expected if CO_2 is strongly nonwetting relative to brine.[18−28] In all cases CO_2 did not imbibe without an applied pressure, i.e. capillary pressure $P_C > 0$, indicating that CO_2 is not wetting or weakly wetting in the CO_2-water system prior to CO_2 contacting the surface. Many of these experiments do not correct for capillary end effects and buoyancy-induced fluid segregation, the lack of which may cause anomalously low values of k_{rc}.[7,8,11,29,30] Critically, none of these experiments present data to show that P_C was sufficiently elevated to ensure S_a^o was achieved. Because capillarity determines pore occupancy based on the smallest pore throat diameter,[7,13,31,32] injecting many pore volumes at a constant CO_2 volumetric flow rate, Q_c, at an insufficient P_C will not achieve S_a^o.[7,8,11] Lower values of maximum k_{rc} may therefore be the result of reduced flow path availability due to any of these three mechanisms, and without data showing that S_a^o was achieved such relative permeability measurements cannot be considered measurements of endpoint CO_2 relative permeability. [Note that some of these articles explicitly state these points and provide data and discussions of these phenomena.] Further details are contained in the Supporting Information.

Pini and Benson[33] presented very similar experiments to those previously performed in this study.[34] k_{rc}^o, P_C, and S_a were measured following the method developed in Ramakrishnan and Cappiello,[35] which stated that S_a could be determined using mass balance, nuclear magnetic resonance imaging (NMR), or X-ray computerized tomographic imaging (X-ray CT). Fordham et al.[36] and Pini et al.[37] demonstrated results with NMR and X-ray CT, respectively. Fordham et al.[36] specifically used NMR imaging with calibrated volume chambers to unambiguously determine saturation profiles using a heavy water-dodecane system and clearly showed the presence of capillary end effects. Pini and Benson[33] used the technique developed in ref 35, taking the derivative of a polynomial fit to the data rather than a derivative of the data or the function suggested by ref 35. Based on the derivative of the polynomial, they report $k_{rc}^o = 0.32$ and 0.92 for gaseous CO_2/brine and supercritical CO_2/brine, respectively, and conclude that CO_2 is strongly nonwetting relative to brine. However, measuring endpoint relative permeability using the technique of ref 35 requires identifying a linear slope of pressure vs flow-rate occurring at several times the entry capillary pressure. More complex data fitting requires carefully choosing a functional form that asymptotes to a straight line. Using only the linear portion of these data (see Figure 2a), we find that $k_{rc}^o = 0.28$ and 0.57 for the gaseous CO_2 and supercritical CO_2 experiments, respectively, indicating that water may not be strongly wetting in a CO_2-water system. Furthermore, their data show higher k_{rc}^o values for supercritical CO_2 than gaseous CO_2, different from what we observe.

In the carbon sequestration literature two common assumptions are followed: (1) the relative permeabilities of the CO_2−H_2O system are that of a CO_2-nonwetting/water-wetting system, and (2) reactions with minerals are driven by the species dissolved in the aqueous phase. The second assumption relies on the ability of the aqueous phase to be in full contact with the grain surface, implying a strongly water-wet system. Previous k_{rc} studies reported relatively low maximum k_{rc} values indicative of a weakly water wetting system. However, with one exception, k_{rc}^o was not directly

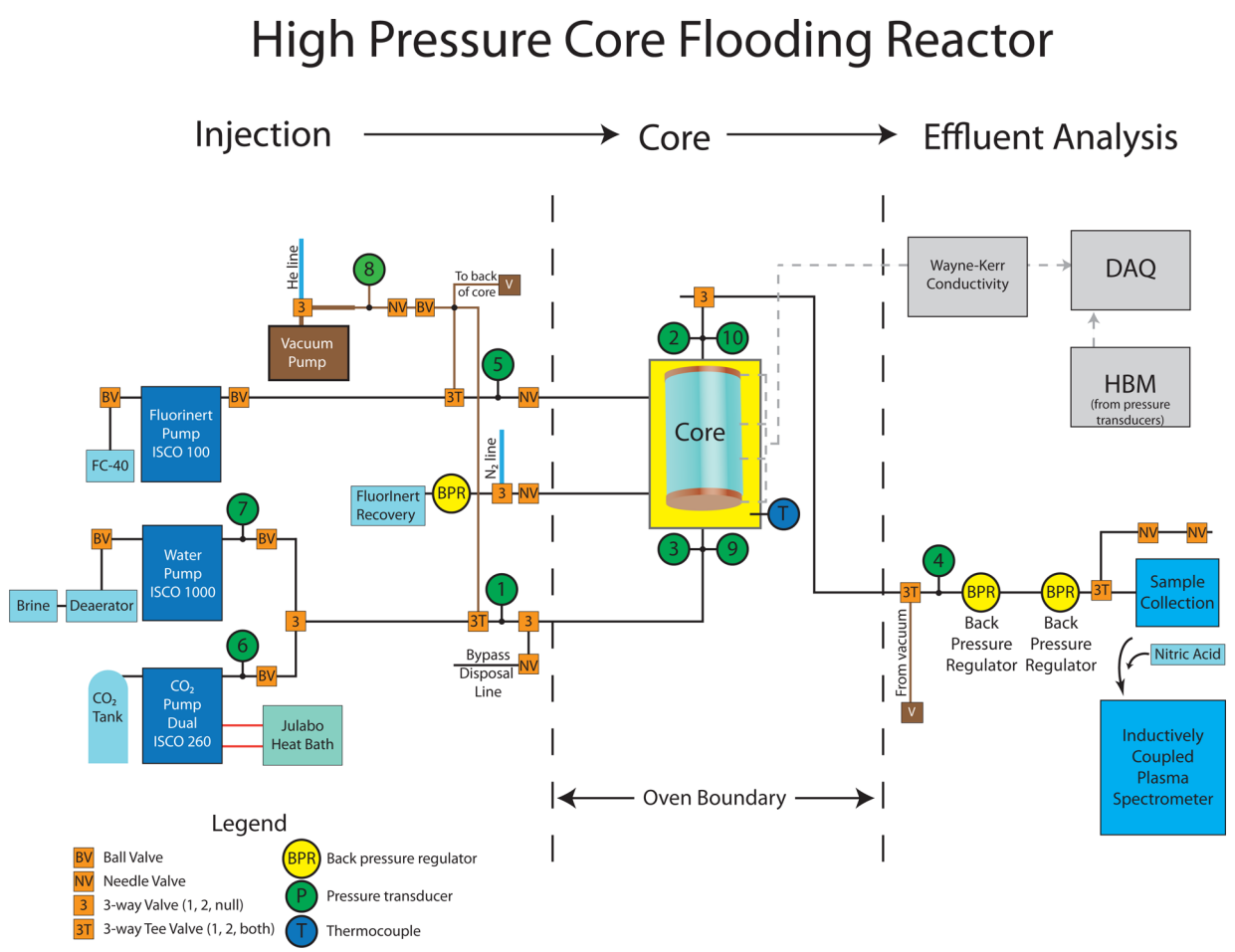

Figure 1. The core flooding system; 1 and 20 MPa transducers are colocated before and after the core. Abbreviations: DAQ = Data Analysis Computer; HBM = HBM pressure signal measurement system.

identified in these studies as per the discussion above. Therefore, we conducted a series of flow-through experiments specifically designed to measure k^o_{rc} in the CO_2-water system. Measurement of k^o_{rc} provides both a qualitative measure of wettability, i.e. pore-scale surface chemistry, as well as a direct measure of the resultant chemistry-induced multiphase fluid conductivity. Due to capillarity-controlled pore-scale fluid occupancy, k_{rc} at all saturations will scale with k^o_{rc}. If CO_2 is strongly nonwetting relative to brine, drainage endpoint CO_2 relative permeability would be expected to be in the range of 0.7−1.

MATERIALS AND METHODS

A schematic of the experimental system developed in ref 34 is shown in Figure 1. Before each experiment, air was evacuated from the system using a two-stage vacuum pump, and deaerated brine was used to saturate the rock. The brine was constituted by mixing 18.2MΩ cm ultrapure water (Millipore Synergy UV) with Fisher Scientific ACS grade NaCl and LiCl salts at a 1000:1 ratio by mass, with LiCl included as a tracer for salt. A two-cylinder piston pump (Isco) for liquid and supercritical CO_2 and a dual reciprocating near pulseless pump (Quizix) for gas phase injection were used to inject CO_2 to displace brine. CO_2 was 99.8% dry (American Gas Products). The core was held vertically in a core holder (Temco) with CO_2 typically displacing brine from the top, though experiments were performed in both directions. Radial stress was applied on a rubber sleeve by pumping Fluorinert (3M) into the surrounding chamber at a controlled pressure, typically 13.7 MPa. Pressure transducers (HBM, 18-bit processing accuracy, 1 MPa: 0.1% full-scale accuracy, 20 MPa: 0.2% full-scale accuracy, simultaneously calibrated with a primary standard dead weight tester with 5 ppm accuracy) were colocated at either end of the core holder to measure the pressure drop across the core for permeability measurements. The core holder and pressure transducers were contained in a temperature-controlled chamber (Watlow) to maintain a constant temperature during each experiment. Four impedance terminals were connected to two current plates that also serve as a fluid distributor and two voltage terminals embedded within the rubber boot. A rough measure of average brine saturation between the voltage terminals could be obtained from resistance data. A pair of back pressure regulators (Tescom) were used to control pressure at the core exit, which in most of the experiments was 10 MPa. The effluent brine and CO_2 were collected in pressurized sampling containers (Swagelok) to provide the average brine saturation in the core by mass balance, which is used to calculate S^o_a (see eq 3 below). All equipment was monitored and controlled by a data acquisition system with a custom-written National Instruments LabView program. CO_2 physical data used in experimental calculations are from NIST,[38] while brine physical data are from ref 39.

dx.doi.org/10.1021/es401549e | Environ. Sci. Technol. 2014, 48, 811−818

Table 1. Endpoint CO_2 Relative Permeability and Average Saturation: Experimental Conditions and Results

Core Properties									Conditions						Results		
Core Material	Length cm	Diameter cm	Porosity %	Brine Perm mD	Std Dev mD	N_2 Perm mD	Std Dev mD	CO_2 Perm mD	Brine	Pressure MPa	Temp °C	CO_2 Properties Phase	Viscosity μPa·s	Density kg/m^3	CO_2 Endpoint Relative Permeability	Corrected CO_2 Endpoint Relative Perm	Endpoint CO_2 Saturation
Berea sandstone																	
Berea 100	10.17	3.8	15.7	116	2.4	190.2	2.0	X	1%	10	20	Liquid	81.5	856	0.44	0.44	0.95
Berea 500	10.28	3.79	24	665	8.1	1090	49	X	5%	10	20	Liquid	81.5	856	0.38	0.38	0.55
Berea 500	10.28	3.8	24	688	4.2	1085	12	X	5%	10	20	Liquid	81.5	856	0.19	0.19	0.60
Berea 500	10.28	3.8	24	688	4.2	1085	12	630	N/A	10	50	SupCrit	28.4	384	X	X	X
Artificial P3C alumina ceramic																	
P3C	10.18	3.9	42.5	12	0.1	20.4	0.4	X	5%	10	20	Liquid	81–84	856–868	0.33	0.34	0.67
P3C	20.75	3.88	42.5	12.2	0.03	20.4	0.4	X	DI	10	20	Liquid	81–86	856–877	0.34	0.36	0.66
P3C	10.17	3.89	42.5	12.8	4.0	20.4	0.4	12.9	DI	10	20	Liquid	81–85	856–872	0.37	0.39	0.63
P3C	10.35	3.78	42.5	12.3	0.1	20.4	0.4	X	DI	10	50	SupCrit	28–33	384–452	0.30	0.35	0.76
P3C	20.75	3.88	42.5	12.1	0.05	20.4	0.4	X	DI	10	50	SupCrit	28–32	384–433	0.37	0.40	0.60
Experiments at lower pressure																	
P3C	20.75	3.89	42.5	11.9	0.3	20.4	0.4	9.8	DI	1.1	20	Gas	14.7–14.9	21–36	0.43	0.51	N/A
P3C	20.75	3.89	42.5	11.9	0.3	20.4	0.4	X	DI	2	20	Gas	15–15.1	41–54	0.55	0.62	N/A
P3C	20.75	3.89	42.5	11.9	0.3	20.4	0.4	X	DI	3.5	20	Gas	15.5–15.9	81–101	0.36	0.43	N/A
P3C	20.75	3.89	42.5	11.9	0.3	20.4	0.4	X	DI	6.5	20	Liquid	70–76	797–830	0.51	0.55	N/A

Cores included Berea sandstone, chosen for its relative homogeneity, and synthetic P3C alumina ceramic (CoorsTek), which is inert to brine, CO_2, and carbonic acid. Cores were prepared to be approximately 4″ in length and 1.5″ in diameter, with the exact dimensions used in calculations. Later experiments were conducted with 8″ length P3C cores to minimize capillary end effects. All cores were vacuum-dried overnight at 70 °C prior to each experiment. Helium intrusion porosity measurements were made on cores that were 1.5″ long and 1.5″ diameter and cored from rock adjacent to the cores used in the experiment. Mercury intrusion porosimetry was previously performed on cores from similar samples and the resulting pore size distribution data used to obtain S_a^o (see below).

Brine permeability was measured at the beginning of each experiment at both atmospheric and experimental pressures by flowing brine at a series of increasing flow rates followed by an identical series of decreasing steps in flow rate at evenly spaced increments, typically 0−20 mL/min in 4 mL/min increments. Permeability was calculated from a least-squares linear fit to the slope of volumetric flow rate vs pressure drop across the core, $\Delta P_{io} \equiv P_i - P_o$, where subscripts i and o denote conditions at the core inlet and outlet, respectively. At least three independent measurements of permeability were made, and their average was reported for each experiment, with similar values at atmospheric and experimental pressures. CO_2 permeability was measured on three cores following the same procedures as those used to measure brine permeability. Brine and CO_2 permeability agreed within variations between independent measurements (see Table 1) given the limits of the equipment and the small ΔP_{io} during CO_2 permeability measurements.

The endpoint CO_2 relative permeability experiments presented here use the technique proposed by ramakrishnan and Cappiello.[35] The advantage of this method is that capillary end effects are automatically removed by considering differential increases in flow rate with respect to ΔP_{io} or equivalently injection pressure. Although the entire k_{rn} curve may be obtained with this method, our emphasis here is the determination of k_{rc}^o. This amounts to obtaining the increase in ΔP_{io} due to an imposed increase in steady-state volumetric flow rate of $CO_2(Q_c)$, at inlet saturations close to S_a^o. Pressure in both phases just outside the outlet of the core must be equal to the wetting phase pressure, here the aqueous phase, in the pores in the outlet face of the core. At steady state $Q_a = 0$ and so, from eq 1, P_a must be constant throughout the core, and thus $P_a = P_o$, the nominal pressure, throughout the core. At the core inlet, $P_{Ci} = P_i - P_a = P_i - P_o = \Delta P_{io}$. The solution for $k_{rc} = \hat{k}_{rc}(P_{Ci})$ and $S_a = \hat{S}_a(P_{Ci})$ as functions (denoted by ^) of inlet capillary pressure, with $P_{Ci} = \Delta P_{io}$ are

$$\hat{k}_{rc}(P_{Ci}) = \frac{L}{A}\frac{\mu_c}{k}\frac{\mathrm{d}Q_c}{\mathrm{d}\Delta P_{io}} \tag{2}$$

$$\hat{S}_a(P_{Ci}) = \frac{L}{A}\frac{\mu_c}{k k_{rc}(P_{Ci})}\frac{\mathrm{d}(Q_c \overline{S}_a)}{\mathrm{d}\Delta P_{io}} \tag{3}$$

where L is core length, A is core area, and $\overline{S}_a$ is the average brine saturation, determined here by effluent mass balance at each steady-state injection rate. Figure 2 shows pressure drop vs flow rate for each experiment, the local slope of which is used to determine k_{rc}^o.

Although mass flux is constant at steady state, volumetric flux increases as pressure decreases from the inlet to the outlet end of the porous medium. Therefore, k_{rc} obtained by the method of ref 35 must be corrected for this volumetric compressibility effect.[40] For an injected steady-state mass flow rate of CO_2, $\dot{m}_i$, at each P_i

$$\hat{k}_{rc}(P_{Ci}) = \frac{L}{A}\frac{\mu_c(P_i)}{k\rho_c(P_i)}\frac{\mathrm{d}\dot{m}_i}{\mathrm{d}\Delta P_{io}} \tag{4}$$

where $\rho_c(P_i)$ is the density at P_i. While the correction is small for liquid CO_2, it is nontrivial for gaseous and supercritical CO_2, see Table 1 below.

Due to capillarity, achieving flow across a core requires a minimum P_i, called the breakthrough pressure P_b, to overcome the P_C for the largest set of pore throat radii that allows for a single flow path across the core. From the Young−Laplace equation, P_C is inversely proportional to pore throat radius, and so increases in P_C relative to P_b will cause the nonwetting CO_2 to invade pores connected by correspondingly decreasing pore throat radii. Therefore, S_a^o was achieved by raising ΔP_{io} above the independently measured P_b[35] by at minimum the ratio of the largest to smallest pore throats as measured by Hg intrusion porosimetry (Figures S1 and S2). Establishment of a constant value of $dQ_c/d\Delta P_{io}$, i.e. a linear slope, at high flow rates confirms that capillarity-determined flow paths, and equivalently pore occupancy, are unchanged and thus that S_a^o was reached at the inlet.

With γ as the interfacial tension between the two fluids, the capillary number $N_C = v_c\mu_c/\gamma$ was about 10^{-8} for these experiments, far below the residual wetting phase mobilization

dx.doi.org/10.1021/es401549e | Environ. Sci. Technol. 2014, 48, 811−818

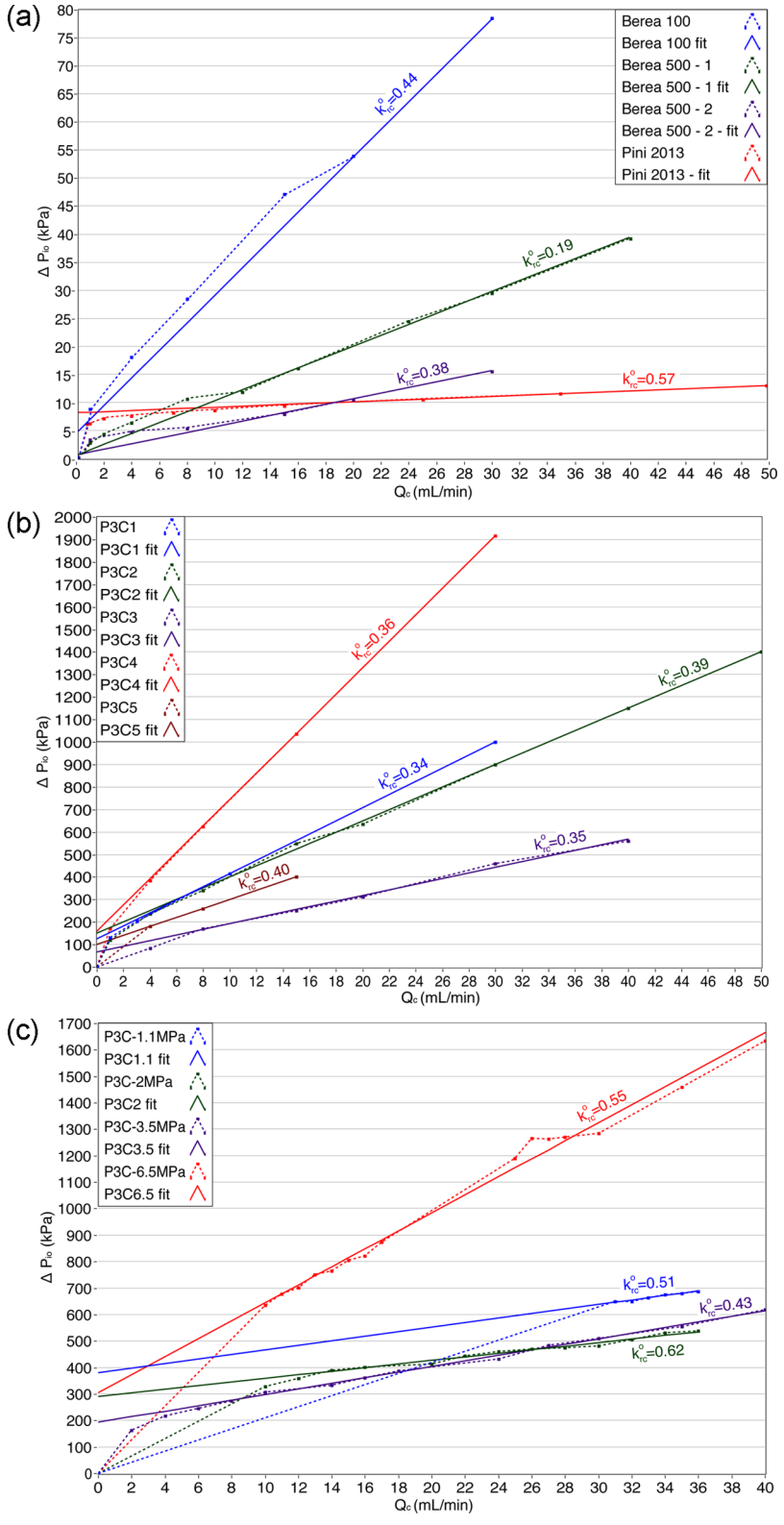

Figure 2. Measured pressure difference as a function of flow rate for (a) Berea sandstone experiments including comparable data from ref 33, (b) P3C experiments at 10 MPa, and (c) P3C experiments at lower pressures indicated in the figure legend. The local slope is used to compute endpoint CO_2 relative permeability. See Table 1 for detailed results; experiments correspond to the labeled k^o_{rc} values shown in the figures.

threshold of about 10^{-3}.[41] Capillarity dominates during core scale CO_2/brine experiments, stabilizing viscous instabilities.[42] Nonetheless, for the sake of robustness initial experiments injected CO_2 into the core from below so that buoyancy and viscous instabilities were reinforced, while later experiments injected CO_2 from above and confirm that the results were largely unchanged.

dx.doi.org/10.1021/es401549e | *Environ. Sci. Technol.* 2014, 48, 811−818

RESULTS AND DISCUSSION

Experimental conditions and results are reported in Table 1, ordered first by core material, then by pressure and temperature and hence CO_2 state. Figure 2 shows the determination of k^o_{rc} from the linear slope of ΔP_{io} vs Q_c at the highest flow rates. Q_c, ΔP_{io}, and $\overline{S}_c$ data are available in the Supporting Information. k^o_{rc} was found to have similar intermediate values at all conditions, ranging from 0.19 to 0.62, but with the majority of results clustered between 0.34 and 0.44. The characteristic convex shape of the plot of ΔP_{io} vs Q_c as well as $P_C > 0$ are indicative of a nonwetting phase intrusion, confirming that CO_2 is the nonwetting phase in comparison to water. Endpoint CO_2 saturation, defined as $1-S^o_a$, was determined from $\overline{S}_a$ measured by mass balance and processed using eq 3 and varied from 0.55 to 0.95 during dense-phase experiments. Impedance-derived saturation measurements (Figures S3 and S4) on the first several cores confirmed the low brine saturations measured from mass balance.

To confirm that the measurements of k^o_{rc} were measuring the desired multiphase flow effects and not an experimental artifact, a number of experimental variations were performed, each designed to confirm that a particular potential source of fundamental experimental design error was not affecting the results. While the earliest experiments were run with a 5% NaCl brine to simulate in situ salinities, later experiments were run with no or low salt to ensure that salt precipitation could not have reduced the intrinsic rock permeability. Experiments were run at gaseous, liquid, and supercritical CO_2 conditions to probe the effect of CO_2 state and to simulate different reservoir conditions. Similarly, to ensure an appropriate baseline permeability for the relative permeability experiments, measurements were made for gaseous, liquid, and supercritical CO_2 permeability on a subset of cores and confirmed that CO_2 permeabilities are in agreement with liquid water permeability (compare brine, CO_2, and N_2 permeabilities in Table 1). To confirm that the relative permeability method handled capillary end effects correctly, the final six P3C experiments used longer 8″ cores with relatively small capillary end effects, with the results substantially the same.

Prior to these experiments, it was anticipated that CO_2 would behave as a strongly nonwetting fluid and that CO_2 drainage endpoint relative permeabilities would therefore be in the range of 0.7−1. Instead, the experiments yielded intermediate values of k^o_{rc}, clustered around 0.35−0.4. The median was 0.39 and the mean was 0.41 with a standard deviation of 0.11, while dense-phase experiments had median and mean k^o_{rc} of 0.38 with a standard deviation of 0.09. High endpoint CO_2 saturations (Berea: 0.55, 0.6, 0.95, P3C: 0.6−0.76) were consistent with typical values for S^o_a from the theoretical literature and were higher than most previously reported saturations from the CO_2 literature, e.g., refs 18−21 with the lowest measurement in agreement with more recent measurements of S^o_a [33] and S_a close to S^o_a.[26,27] While the results might appear to be independent of system conditions, with perhaps the exception of the gas phase results, such a conclusion would require a more systematic set of experiments to probe sensitivity to each variable.

H_2O is slightly soluble in dense-phase CO_2, and, therefore, residual water will evaporate into the flowing CO_2, slowly increasing k_{rc}.[17] Our results during the extended CO_2 flowing period did not indicate a gradual increase in k_{rc}, probably because of the relatively short time-scale of each experiment. Berg et al.[28] found negligible differences in $\overline{S}_a$ between unsaturated and saturated drainage experiments due to the limited solubility of water into CO_2. However, they also report subcore scale differences in saturation profiles, though with too many experimental design differences to be able to draw any conclusions with respect to this work.

Water evaporation may also cause salt precipitation. Since salt occupies a fraction of the volume occupied by water (at most 2% in our experiments), and its precipitation is likely to occur on the trailing edge of the displacement front, we do not expect halite formation to be the cause of the reduction in endpoint permeability. This is further confirmed by the experiments conducted with deionized water in synthetic media with little difference in the results between 5% salt and deionized water. Reduced intrinsic permeability due to chemical rearrangement of the pore network cannot explain the results as both the synthetic alumina and sandstone cores studied are relatively inert and further reinforced by results that are similar in both media.

Our experimental measurements suggest endpoint CO_2 relative permeabilities that are smaller by about a factor of 2 than those expected for a strongly water-wetting system and are possibly reflective of a weakly water-wetting system, especially when dense CO_2 is the injected fluid. When the same experiment was conducted with N_2, an endpoint relative permeability closer to unity was obtained. Further experiments are necessary to confirm or refute the wettability hypothesis, which should include more complex lithologies than the relatively homogeneous and inert synthetic P3C alumina and Berea sandstone cores studied here.

The chemistry of CO_2, brine, and mineral surfaces has proven to be complex. Typically low contact angles, in the 20−40° range,[43−45] conflict with reports of higher contact angles in the 50−70° range at higher pressures and ionic strengths.[46] Flow-through experiments in glass micromodels suggest that CO_2−H_2O systems may be weakly water wetting or intermediate wetting at pressures and temperatures similar to those in this study.[47,48] Similarly, molecular simulations show aqueous phase CO_2 reactions driving surface reactivity,[49] i.e. CO_2 does not simply behave as an inert fluid and alters the system wettability. The results here point to the continuing need for further pore- and molecular-scale experimental data on transport and surface chemistry processes, with a particular need to understand the dynamics of CO_2 and thin brine films, e.g., ref 50.

Implications for Geologic Carbon Sequestration. For a fixed injection pressure, halving the endpoint CO_2 relative permeability from the expected range of 0.7−1 will cause a proportional decrease in CO_2 injectivity, discussed above and also shown by displacement models.[17] CO_2 reservoirs limited by the fracturing pressure of the overlying caprock, e.g., refs 14 and 51, will have decreased disposal capacity. By contrast, because plume spreading occurs with respect to a characteristic migration advective velocity which is directly proportional to λ_c,[16] CO_2 reservoirs limited by areal extent will have increased disposal capacity. A reduction in CO_2 mobility may also stabilize plume fronts, as similar analyses have shown for water flooding in oil reservoirs.[7] A variety of indirect effects, including plume evolution and residual capillary trapping, may also be linked to mobility.[52]

Future petrophysical analyses for potential CO_2 sequestration sites should include relative permeability measurements on reservoir core samples rather than relying on extrapolations based on prior studies. Based on these results, CO_2 injectivity

will be reduced and pressure-limited reservoirs will have reduced disposal capacity, though area-limited reservoirs may have increased capacity. Assuming the majority of reservoirs are pressure limited, and if the experimental results reported here are found to apply to other lithologies as well, geologic carbon sequestration at scale will require about twice the number of disposal sites and/or wells.

■ ASSOCIATED CONTENT

Supporting Information

Tabulated numerical results for each experiment (Q_c, ΔP_{io}, $\overline{S}_a$), mercury intrusion porosimetry data, and resistivity-derived local saturation data. This material is available free of charge via the Internet at http://pubs.acs.org.

■ AUTHOR INFORMATION

Corresponding Author

*E-mail: jonathan.levine@netl.doe.gov. Phone: 412-386-7534. Fax: 412-386-4604.

Present Addresses

[§]National Energy Technology Laboratory, Pittsburgh, PA 15236.

[∥]Ocean and Earth Science, University of Southampton, UK.

Notes

The authors declare the following competing financial interest(s): Schlumberger has a carbon service business.

■ ACKNOWLEDGMENTS

J.L. acknowledges the entire CO_2 research group at Schlumberger-Doll Research for help with experiments as well as helpful discussions. This work was supported by a NYSERDA grant (NYSERDA-10113), and J.L. acknowledges support from the U.S. National Science Foundation, through a Fellowship in the IGERT Joint Program in Applied Mathematics and Earth and Environmental Science at Columbia University. The manuscript was greatly improved thanks to the comments and feedback received from the reviewers.

■ NOMENCLATURE

k	permeability
$\hat{k}_{rj}(S_j)$	relative permeability of phase j, which is a function of the saturation of phase j
k^o_{rj}	endpoint relative permeability of phase j
$\dot{m}_j$	mass flow rate of phase j
v_j	velocity of phase j
A	area
L	length
N_C	capillary number
ΔP_{io}	pressure difference between the inlet and outlet of the core
P_b	breakthrough pressure
P_C	capillary pressure
P_j	pressure, phase j or location: i = inlet, o =outlet
Q_j	volumetric flow rate of phase j
$\overline{S}_j$	average saturation of phase j
S_j	saturation of phase j
S^o_j	residual saturation of phase j
γ	interfacial tension
λ_j	mobility of phase j; $\lambda_j = kk_{rj}/\mu_j$
μ_j	shear coefficient of viscosity of phase j
ρ_j	density of phase j

Subscripts

a	aqueous phase
c	CO_2 phase
C	capillary, either capillary pressure or capillary number
d	phase being displaced
i	core inlet
j	phase j
n	nonwetting phase
o	core outlet
w	wetting phase

■ REFERENCES

(1) *Fuels decarbonization and carbon sequestration: report of a workshop*; Socolow, R., Ed.; 1997.

(2) *IPCC Special Report on Carbon Dioxide Capture and Storage*; Metz, B., Davidson, O., de Coninck, H., Loos, M., Meyer, L., Eds.; 2005.

(3) Levine, J. S.; Matter, J. M.; Goldberg, D. S.; Cook, A.; Lackner, K. S. Gravitational trapping of carbon dioxide in deep sea sediments: Permeability, buoyancy, and geomechanical analysis. *Geophys. Res. Lett.* **2007**, *34*.

(4) Goldberg, D. S.; Takahashi, T.; Slagle, A. L. Carbon dioxide sequestration in deep-sea basalt. *Proc. Natl. Acad. Sci.* **2008**, *105*, 9920.

(5) Koide, H.; Shindo, Y.; Tazaki, Y.; Iijima, M.; Ito, K.; Kimura, N.; Omata, K. Deep sub-seabed disposal of CO2—The most protective storage. *Energy Convers. Manage.* **1997**, *38*, 253–258.

(6) Leverett, M. C. Flow of oil-water mixtures through unconsolidated sands. *Trans. AIME* **1939**, *132*, 149–171.

(7) Willhite, G. P. *Waterflooding*; Society of Petroleum Engineers: Richardson, TX, 1986.

(8) Anderson, W. Wettability literature survey part 5: The effects of wettability on relative permeability. *J. Pet. Technol.* **1987**, *39*, 1453–1468.

(9) Corey, A. T. The interrelation between gas and oil relative permeabilities. *Prod. Mon.* **1954**, *19*, 38–41.

(10) Land, C. Calculation of imbibition relative permeability for two- and three-phase flow from rock properties. *SPE J.* **1968**, *8*, 149–156.

(11) Honarpour, M.; Koederitz, L.; Harvey, A. *Relative permeability of petroleum reservoirs*; CRC Press Inc.: Boca Raton, FL, 1986.

(12) Lake, L. W. *Enhanced Oil Recovery*; Prentice Hall: 1989.

(13) Ramakrishnan, T. S.; Wasan, D. T. Effect of capillary number on the relative permeability function for two-phase flow in porous media. *Powder Technol.* **1986**, *48*, 99–124.

(14) Lucier, A.; Zoback, M.; Gupta, N.; Ramakrishnan, T. S. Geomechanical aspects of CO2 sequestration in a deep saline reservoir in the Ohio River Valley region. *Environ. Geosci.* **2006**, *13*, 85.

(15) Hesse, M. A.; Orr, F. M.; Tchelepi, H. A. Gravity currents with residual trapping. *J. Fluid Mech.* **2008**, *611*, 35–60.

(16) de Loubens, R.; Ramakrishnan, T. S. Analysis and computation of gravity induced migration in porous media. *J. Fluid Mech.* **2011**, *675*, 60–86.

(17) Kopp, A.; Class, H.; Helmig, R. Investigations on CO2 storage capacity in saline aquifers-Part 2: Estimation of storage capacity coefficients. *Int. J. Greenhouse Gas Control* **2009**, *3*, 277–287.

(18) Bachu, S.; Bennion, B. Effects of in situ conditions on relative permeability characteristics of CO2-brine systems. *Environ. Geol.* **2008**, *54*, 1707–1722.

(19) Bennion, B.; Bachu, S. Drainage and imbibition CO2/brine relative permeability curves at reservoir conditions for carbonate formations, SPE 134028. *SPE Annual technical conference and exhibition, Florence, Italy, Society of Petroleum Engineers*, 2010.

(20) Bachu, S. Drainage and imbibition CO2/brine relative permeability curves at in situ conditions for sandstone formations in western Canada. *Energy Procedia* **2013**,

(21) Perrin, J. C.; Benson, S. An experimental study on the influence of sub-core scale heterogeneities on CO2 distribution in reservoir rocks. *Transp. Porous Media* **2010**, *82*, 93–109.

(22) Krevor, S.; Pini, R.; Zuo, L.; Benson, S. M. Relative permeability and trapping of CO2 and water in sandstone rocks at reservoir conditions. *Water Resour. Res.* **2012**, *48*.
(23) Zuo, L.; Krevor, S.; Falta, R. W.; Benson, S. M. An experimental study of CO2 exsolution and elative permeability measurements during CO2 saturated water depressurization. *Transp. Porous Media* **2012**, *91*, 459−478.
(24) Shi, J.-Q.; Xue, Z.; Durucan, S. Supercritical CO2 core flooding and imbibition in Tako sandstone- Influence of sub-core scale heterogeneity. *Int. J. Greenhouse Gas Control* **2011**, *5*, 75−87.
(25) Suekane, T.; Nobuso, T.; Hirai, S.; Kiyota, M. Geological storage of carbon dioxide by residual gas and solubility trapping. *Int. J. Greenhouse Gas Control* **2008**, *2*, 58−64.
(26) Chang, C.; Zhou, Q.; Xia, L.; Li, X.; Yu, Q. Dynamic displacement and non-equilibrium dissolution of supercritical CO2 in low-permeability sandstone: An experimental study. *Int. J. Greenhouse Gas Control* **2013**, *14*, 1−14.
(27) Akbarabadi, M.; Piri, M. Relative permeability hysteresis and capillary trapping characteristics of supercritical CO2/brine systems: an experimental study at reservoir conditions. *Adv. Water Resour.* **2012**,
(28) Berg, S.; Oedai, S.; Ott, H. Displacement and mass transfer between saturated and unsaturated CO_2−brine systems in sandstone. *Int. J. Greenhouse Gas Control* **2013**, *12*, 478−492.
(29) Rappaport, L. A.; Leas, W. J. Properties of linear waterfloods. *Trans. AIME* **1953**, *198*, 139.
(30) Huang, D. D.; Honarpour, M. M. Capillary end effects in coreflood calculations. *J. Pet. Sci. Eng.* **1998**, *19*, 103−117.
(31) Dullien, F. A. L.; Dhawan, G. K. Bivariate pore-size distributions of some sandstones. *J. Colloid Interface Sci.* **1975**, *52*, 129−135.
(32) Wilkinson, D. Percolation effects in immiscible displacement. *Phys. Rev. A* **1986**, *34*, 1380−1391.
(33) Pini, R.; Benson, S. M. Simultaneous determination of capillary pressure and relative permeability curves from core-flooding experiments with various fluid pairs. *Water Resour. Res.* **2013**,10.1002/wrcr.20274.
(34) Levine, J. S. Relative permeability experiments of carbon dioxide displacing water & their implications for carbon sequestration. Ph.D. Thesis, Columbia University, 2011.
(35) Ramakrishnan, T. S.; Cappiello, A. A new technique to measure static and dynamic properties of a partially saturated porous medium. *Chem. Eng. sci.* **1991**, *46*, 1157−1163.
(36) Fordham, E. J.; Hall, L. D.; Ramakrishnan, T. S.; Sharpe, M. R.; Hall, C. Saturation gradients in drainage of porous media: NMR imaging measurements. *AIChE J.* **1993**, *39*, 1431−1443.
(37) Pini, R.; Krevor, S.; Benson, S. M. Capillary pressure and heterogeneity for the CO2/water system in sandstone rocks at reservoir conditions. *Adv. Water Resour.* **2012**, *38*, 48−59.
(38) Lemmon, E. W.; McLinden, M. O.; Friend, D. G. Thermophysical Properties of Fluid Systems. *NIST Chemistry WebBook* **2010**, *NIST Standard Reference Database*.
(39) Lide, D. R. *CRC Handbook of Chemistry and Physics* (Internet version 2010); CRC: Boca Raton, FL, 2010.
(40) Ramakrishnan, T. S.; Chugunov, N. Compressibility corrections to relative permeability from the non-uniform steady-state method. *Chem. Eng. Sci.* **2013**, 73−77.
(41) Dombrowski, H. S.; Brownell, L. E. Residual equilibrium saturation of porous media. *Ind. Eng. Chem.* **1954**, *46*, 1207−1219.
(42) Berg, S.; Ott, H. Stability of CO2−brine immiscible displacement. *Int. J. Greenhouse Gas Control* **2012**, *11*, 188−203.
(43) Espinoza, D. N.; Santamarina, J. C. Water-CO2-mineral systems: Interfacial tension, contact angle, and diffusion−Implications to CO2 geological storage. *Water Resour. Res.* **2010**, *46*, W07537.
(44) Wang, S.; Edwards, I. M.; Clarens, A. F. Wettability phenomena at the co2−brine−mineral interface: Implications for geologic carbon sequestration. *Environ. Sci. Technol.* **2012**, *47*, 234−241.
(45) Broseta, D.; Tonnet, N.; Shah, V. Are rocks still water-wet in the presence of dense CO2 or H2S? *Geofluids* **2012**, *12*, 280−294.
(46) Jung, J.-W.; Wan, J. Supercritical CO2 and ionic strength effects on wettability of silica urfaces: Equilibrium contact angle measurements. *Energy Fuels* **2012**, *26*, 6053−6059.
(47) Chalbaud, C.; Lombard, J. M.; Martin, F.; Robin, M.; Bertin, H.; Egermann, P. Two phase flow properties of brine-CO2 systems in a carbonate core: Influence of wettability on Pc and kr. *SPE/EAGE Reservoir Characterization and Simulation Conference* **2007**.
(48) Kim, Y.; Wan, J.; Kneafsey, T. J.; Tokunaga, T. K. Dewetting of silica surfaces upon reactions with supercritical CO2 and brine: pore-scale studies in micromodels. *Environ. Sci. Technol.* **2012**, *46*, 4228−4235.
(49) Iglauer, S.; Mathew, M.; Bresme, F. Molecular dynamics computations of brine-CO2 interfacial tensions and brine-CO2-quartz contact angles and their effects on structural and residual trapping mechanisms in carbon geo-sequestration. *J. Colloid Interface Sci.* **2012**,
(50) Kim, T. W.; Tokunaga, T. K.; Bargar, J. R.; Latimer, M. J.;Webb, S. M. Brine film thicknesses on mica surfaces under geologic CO2 sequestration conditions and controlled capillary pressures. *Water Resour. Res.* **2013**,
(51) Stauffer, P. H.; Viswanathan, H. S.; Pawar, R. J.; Guthrie, G. D. A system model for geologic sequestration of carbon dioxide. *Environ. Sci. Technol.* **2008**, *43*, 565−570.
(52) Altundas, B.; Ramakrishnan, T. S.; Chugunov, N.; de Loubens, R. Retardation of CO2 migration due to capillary pressure hysteresis: A new CO2 trapping mechanism. *Soc. Pet. Eng. J.* **2011**, *16*, 784−794.